2012 IEEE International Conference on Robotics and Automation
RiverCentre, Saint Paul, Minnesota, USA
May 14-18, 2012

Motion Control of *Tetrahymena pyriformis* Cells with Artificial Magnetotaxis: Model Predictive Control (MPC) Approach

Yan Ou[1], Dal Hyung Kim[2], Paul Kim[2], Min Jun Kim[2], A. Agung Julius[1]

Abstract— **The use of live microbial cells as microscale robots is an attractive premise, primarily because they are easy to produce and to fuel. In this paper, we study the motion control of magnetotactic *Tetrahymena pyriformis* cells. Magnetotactic *T. pyriformis* is produced by introducing artificial magnetic dipole into the cells. Subsequently, they can be steered by using an external magnetic field. We observe that the external magnetic field can only be used to affect the swimming direction of the cells, while the swimming velocity depends largely on the cells' own propulsion. Feedback information for control is obtained from a computer vision system that tracks the cell. The contribution of this paper is twofold. First, we construct a discrete-time model for the cell dynamics that is based on first principle. Subsequently, we identify the model parameters using the Least Squares approach. Second, we formulate a model predictive approach for feedback control of magnetotactic *T. pyriformis*. Both the model fitness and the performance of the feedback controller are verified using experimental data.**

Keywords: magnetotaxis, microrobots, model predictive control, motion control, *Tetrahymena pyriformis*.

I. INTRODUCTION

Microrobots have been widely investigated for many applications, for example, in parallel assembly [1] and micromanipulation [2]. Among those works, most focus on developing artificial microrobots [3], [4], which are relatively easy to control. However, there are two main challenges: one is the high-cost, and another is the limitation in supplying sufficient power for microrobots in a microfludic environment.

There is an increasing number of scholars who focus on utilizing live microorganisms, such as *S. marcescens* and *Tetrahymena pyriformis*, as microrobots, which are called microbiorobots. Microbiorobots are easy and cheap to produce [5]. The biomolecular motors, such as flagella and cilia, embedded in the microorganisms generate swimming forces by consuming chemical energy from fluidic environments. Many existing results focus on controlling prokaryotic cells as microbiorobots. For example, Martel *et al* [6] used magnetotactic bacteria to manipulate micro-objects. Behkam *et al* [7] investigated the random behavior of flagellated bacteria as propulsion units, while Julius *et al* [5] developed a model of a microstructure blotted with bacteria moving in a micro channel propelled by the flagella of the bacteria.

[1]Yan Ou and A. Agung Julius are with the Department of Electrical, Computer, and Systems Engineering, Rensselaer Polytechnic Institute, Troy, NY 12180, Email: ouy2@rpi.edu, agung@ecse.rpi.edu.

[2]Dal Hyung Kim, Paul Kim, and Min Jun Kim are with the Department of Mechanical Engineering and Mechanics, Drexel University, Philadelphia, PA 19104. Email: dk434@drexel.edu, psk25@drexel.edu, mkim@coe.drexel.edu.

On the other hand, some scholars focus on the motion control of the eukaryotic cell [8], [9]. Normally, the size of the eukaryotic cell is much larger than the prokaryotic cell, which makes it easier for us to generate the plant model and capture the positions of a single eukaryotic cell. Whitesides *et al* [10] demonstrated the biological propulsion of microscale loads by the unicellular photosynthetic algae *Chlamydomonas reinhardtii*. Itoh *et al* [11] performed motion control of Euglena group by weak laser scanning system and object manipulation using Euglena group. Kim *et al* [12] showed the usage of galvanotactic and phototactic to control *T. pyriformis* as a microfluidic workhorse. Kim *et al* [13] used real-time feedback control and the rapidly-exploring random tree (RRT) for path planning to control the magnetotactic *T. pyriformis* as a microbiorobot. Even though those works have led to some good motion control performances, the precise plant model for the cell motion and the advanced control technique, which based on the plant model, have not been fully developed.

In this paper, we use the Model Predictive Control (MPC) algorithm [14] to control the magnetotactic *T. pyriformis* as a microbiorobot based on a discrete-time plant model. The research reported in this paper follows our previous work [13] and has two main contributions: First, we construct the discrete-time plant model and calculate the plant model parameters by using the Batch Least Squares (BLS) method. Second, we use the feedback control with MPC algorithm to make *T. pyriformis* follow a predefined track by only changing the angle of the magnetic field. In both cases, the theoretical results are backed by the experimental validations.

II. EXPERIMENTAL SETUP

The same setup is used and reported in our earlier work [13].

A. Cell culture

T. pyriformis is a eukaryotic pear-shaped cell with size 50 μm long and 25 μm wide. The body of *T. pyriformis* is covered by approximately 600 cilia, both oral and locomotive. The locomotive cilia facilitate the swimming behavior of *T. pyriformis* which can be effectively influenced by the magnetotaxis [15]. *T. pyriformis* is cultured in the appropriate culture medium [13]. The saturated culture has 10^4 cell·ml^{-1} of the cell density. The cell culture medium is diluted with a fresh culture medium in a $1:3$ ratio (working cell density is $3.3 \cdot 10^3$ cells·ml^{-1}) in order to lower the cell concentration for the single cell detection.

B. Fabrication of artificially magnetotactic T. pyriformis

Figure 1 shows the process to create the artificially magnetotactic *T. pyriformis*. In Figure 1 (a), 0.1% iron-oxide spherical particles with diameter $50nm$ are added into the culture medium. In Figure 1 (b), the culture medium with iron-oxide particles is gently agitated and left for about 10 minutes to ensure sufficient internalization of the magnetite. Based on the image we get, the average volume of the amount of internalization of each cell is about $500\mu m^3$. However, it varies a lot among cells. The swimming behavior of the magnetite loaded *T. pyriformis* is identical to the normal cell [16]. Figure 1 (c) shows that a permanent magnet is applied around the cell culture for about one minute to magnetize the internalized magnetite. After magnetization, *T. pyriformis* swims freely without the external magnetic field. Kim *et al* [15] has empirically observed that the magnetites are always aligned with the major axis of the cell. The strength of the magnetic dipoles remains nearly constant for over one hour even after the permanent magnet is removed after magnetization; therefore, it is assumed that the internalized magnetite is saturated during experiments [15].

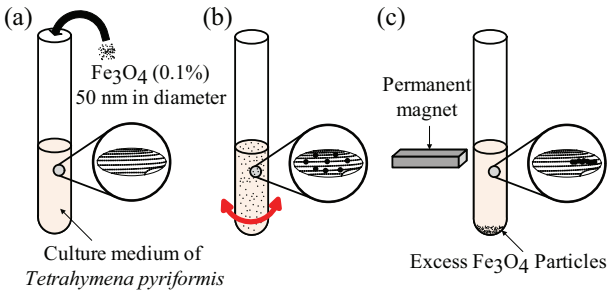

Fig. 1: [13] The procedure for fabrication of artificially magnetotactic *T. pyriformis* from (a) to (c). (a) Addition of iron oxide particles (magnetite, Fe_3O_4) into the culture medium. (b) Gentle agitation to ensure cells internalize iron oxide particles. (c) Magnetization of the internalized magnetite using a permanent magnet.

C. Close loop system

The system shown in Figure 2 (a) is used for feedback control of the magnetotactic *T. pyriformis*, which includes a microscope, a camera, a computer, a control board, two power supplies, and a set of approximate Helmholtz coils. The camera is used to capture images of cell motion. The computer is used to operate image processing and control algorithm. The control board and the power supplies provide power to the approximate Helmholtz coils to generate a magnetic field in a $2D$ system. The field of view through the microscope is limited to 2 mm for each axis. In this field of view, the magnetic field is approximately constant [13]. We use a 640 px by 512 px video with 1 px ≈ 2.32 μm to record the experiment process in this field of view. Figure 2 (b) illustrates the control block diagram.

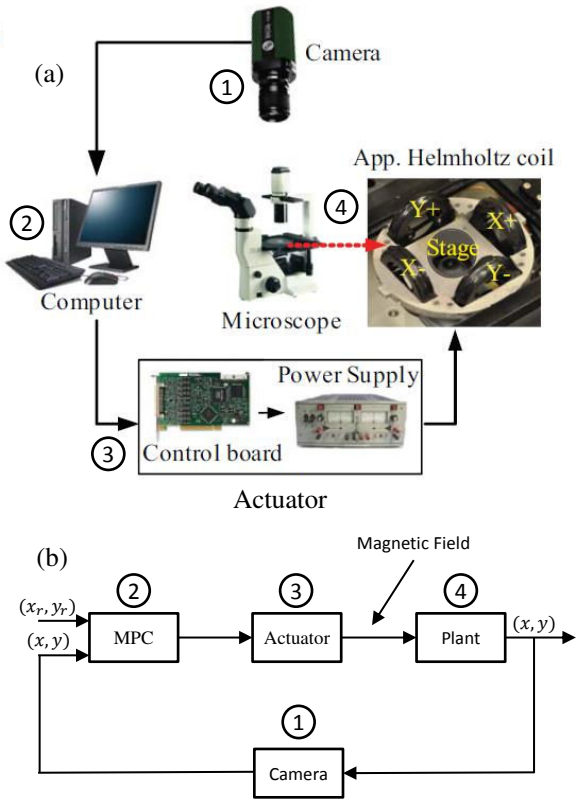

Fig. 2: (a) The experiment setup for the feedback control. (b) Control block diagram [13]. In this picture, (x_r, y_r) is the set point while (x, y) is the cell position.

III. PLANT MODEL

A. Structure of model

Once we exert the magnetic field, the angular difference between the internalized magnetites and the magnetic field will produce a torque on *T. pyriformis* to change the moving direction and lead the cell to align with the magnetic field [15]. Meanwhile, we have empirically discovered that the swimming velocity of the cell does not vary a lot with the intensity of the external magnetic field, which can be shown from Table I.

	T. pyriformis I	*T. pyriformis* II
$\|\mathbf{B}\| = 1$ mT	$\nu_{avg} = 661.9749\ \mu m{\cdot}s^{-1}$	$\nu_{avg} = 863.7337\ \mu m{\cdot}s^{-1}$
$\|\mathbf{B}\| = 1.5$ mT	$\nu_{avg} = 675.1826\ \mu m{\cdot}s^{-1}$	$\nu_{avg} = 868.3528\ \mu m{\cdot}s^{-1}$
$\|\mathbf{B}\| = 2$ mT	$\nu_{avg} = 676.1338\ \mu m{\cdot}s^{-1}$	$\nu_{avg} = 880.3890\ \mu m{\cdot}s^{-1}$
$\|\mathbf{B}\| = 2.5$ mT	$\nu_{avg} = 689.9494\ \mu m{\cdot}s^{-1}$	$\nu_{avg} = 848.9808\ \mu m{\cdot}s^{-1}$

TABLE I: Average velocity of different *T. pyriformis* under the influence of different magnetic field strengths. In this table, $\|\mathbf{B}\|$ is the magnetic field strength; ν_{avg} is the average cell velocity.

Figure 3 shows the mechanical analysis of *T. pyriformis* under the influence of the magnetic field. In this paper, we

keep the strength of magnetic field at a constant level while changing the angle of magnetic field to control *T. pyriformis*. Our experiment is performed in a low Reynolds number fluidic environment. Therefore, the inertia effect is negligible, i.e. the relationship between the torque and the cell angle is approximately linear. The continuous-time plant model is as follows.

$$\tau = \mathbf{m} \times \mathbf{B} = \|\mathbf{m}\|\|\mathbf{B}\| \sin(\theta_t - \theta_m) = -\gamma \dot{\theta}_t, \quad (1)$$

where γ is a constant number; $\|m\|$ is the norm of the magnetic moment; $\|B\|$ is magnetic field strength; τ is the torque generated by the magnetic field and the magnetic moment; θ_t is the cell angle; θ_m is the magnetic field angle. Then, we discretize the continuous-time plant model and derive the following discrete-time equations.

$$\theta_t(k) = a_0\theta_t(k-1) + b_0 \sin(\theta_m(k-1) - \theta_t(k-1)), \quad (2)$$
$$x(k) = x(k-1) + \nu(k)\cos(\theta_t(k)), \quad (3)$$
$$y(k) = y(k-1) + \nu(k)\sin(\theta_t(k)), \quad (4)$$

where k represents the time step; $\nu(k)$ is the cell position distance between two consecutive sampling time, which is almost constant and can be approximately calculated by averaging the previous 10 steps' cell velocity; a_0 and b_0 are constant for each individual cell; $\hat{a}_0 \approx 1$ in most experimental results; b_0 represents cell's angular changing rate with respect to the magnetic field; a_0 and b_0 vary for different cells due to different cell features and the amount of iron particles internalization; $(x(k-1), y(k-1))$ and $(x(k), y(k))$ are cell positions.

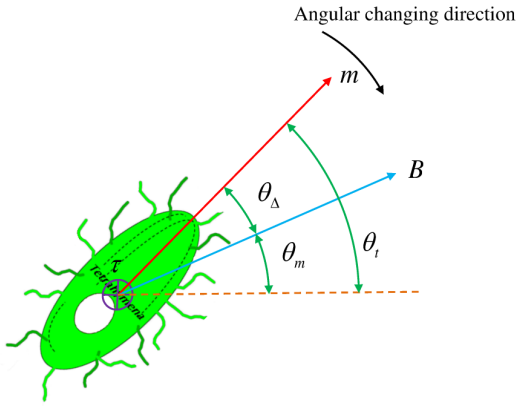

Fig. 3: Mechanical analysis of the magnetized *T. pyriformis* under the influence of magnetic field. In this picture, $\mathbf{B}$ is the magnetic field; $\mathbf{m}$ is the magnetic moment; τ is the torque generated from $\mathbf{B}$ and $\mathbf{m}$; θ_t is the cell angle; θ_m is the magnetic field angle; $\theta_\Delta = \theta_t - \theta_m$.

B. Parameter identification

To get the plant parameters a_0 and b_0, we conduct experiments for manual control in a polydimethylsiloxane (PDMS) channel. The PDMS channel is fabricated with depth of 80 μm to give cells sufficient space for freely swimming. The magnetic field is manually changed by positive and negative directions on either the x-axis or y-axis with the four array keys on the keyboard. In the experiments, the sampling time is 10 frames per second. We manually rotate the magnetic field 90 degrees each time while keeping the strength of magnetic field at a constant level. Based on the discrete-time plant model (2)-(4) and the manual control data, BLS method can be used to identify the plant parameters a_0 and b_0. To ensure the convergence of a_0 and b_0, it is necessary to consider the Persistent Excitation (PE) issue that the input signal should contain enough frequencies [17]. In this case, we choose a nonperiodic rectangular wave as input. Then, we collect the input and output data, $\theta_m(0), \theta_m(1), \ldots, \theta_m(k), \ldots, \theta_m(n)$, and $\theta_t(0), \theta_t(1), \ldots, \theta_t(k), \ldots, \theta_t(n)$ and derive the following equation based on Equation (2).

$$\begin{bmatrix} \theta_t(1) \\ \theta_t(2) \\ \vdots \\ \theta_t(k) \\ \vdots \\ \theta_t(n) \end{bmatrix} = \begin{bmatrix} \theta_t(0) & \sin(\theta_m(0) - \theta_t(0)) \\ \theta_t(1) & \sin(\theta_m(1) - \theta_t(1)) \\ \vdots & \vdots \\ \theta_t(k-1) & \sin(\theta_m(k-1) - \theta_t(k-1)) \\ \vdots & \vdots \\ \theta_t(n-1) & \sin(\theta_m(n-1) - \theta_t(n-1)) \end{bmatrix} \begin{bmatrix} a_0 \\ b_0 \end{bmatrix}. \quad (5)$$

Let us rewrite this equation by $Y = \Phi\theta$. Then, based on the BLS method, the best fit parameters are given by $\hat{\theta} = \Phi^\dagger Y$, where $\Phi^\dagger = (\Phi^T\Phi)^{-1}\Phi^T$ is the pseudoinverse of Φ. The estimated outputs $\hat{Y}$ can be expressed by $\hat{Y} \triangleq \Phi\hat{\theta}$.

From one experimental result, as shown in Figure 4, we obtain the optimal parameters $\hat{a}_0 = 1.0000$ and $\hat{b}_0 = 0.4178$. The magnetic field strength is set to be 2 mT. Analytically, we can compute $\cos\alpha$, where α is the angular difference between Y and $\hat{Y}$ as follows.

$$\cos\alpha = \frac{\langle Y, \hat{Y} \rangle}{\|Y\|\|\hat{Y}\|} = \frac{\|\hat{Y}\|}{\|Y\|} \approx 0.9999. \quad (6)$$

This result shows the good fit between the estimated outputs and the experimental outputs.

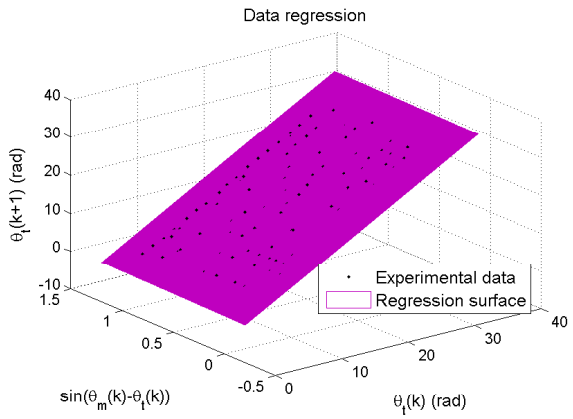

Fig. 4: The data regression of Equation (2). In this picture, the flat purple surface is the regression surface; the black dots are the experimental data.

IV. MPC CONTROLLER DESIGN

A. Path generation method

To test the effectiveness of the controller, we try to make *T. pyriformis* follow a reference track counterclockwise. This track is made up by two lines and two semi-circles, as shown in Figure 5. During each sampling period, two set points $(x_r(k+1), y_r(k+1))$ and $(x_r(k+2), y_r(k+2))$ are generated consecutively based on the current cell position. There exists a constraint for the change of cell angle based on Equation (2).

$$a_0\theta_t(k-1) - b_0 \leq \theta_t(k) \leq a_0\theta_t(k-1) + b_0. \quad (7)$$

Therefore, in order to make *T. pyriformis* follow the reference track while satisfying the constraint, the set points should be generated with a smooth angular changing rate. Figure 5 shows a heuristic method that deal with the three typical cases in the process of generating the set points. **Case I**: $d_1 < 0.2\nu(k)$. The next set point can be located on the reference track with distance $\nu(k)$ from the current cell position. **Case II**: $d_2 > 0.2\nu(k)$ and the cell is inside the reference track. We choose a position, ξ on the reference track, such that the distance from ξ to the current cell position is $\nu(k) + 2d_2$. Then we locate the next set point along the path from the current cell position to ξ with distance $\nu(k)$ from the current cell position. **Case III**: $d_3 > 0.2\nu(k)$ and the cell is outside the reference track. We generate a tangent line from the current cell position to the reference track. Then we locate the next set point along the tangent line to the reference track with distance $\nu(k)$ from the current cell position. However, if the cell's angular changing rate b_0 is too small, the generated set point still does not satisfy the constraint, i.e. $\theta_t(k) < a_0\theta_t(k-1) - b_0$ or $\theta_t(k) > a_0\theta_t(k-1) + b_0$. We can choose $\theta_t(k) = a_0\theta_t(k-1) - b_0$ or $\theta_t(k) = a_0\theta_t(k-1) + b_0$ and recompute the set point.

B. MPC algorithm

MPC is an advanced control technique mostly applied in the process industries [14], such as chemical plants and oil refineries. Here we apply the MPC algorithm to the motion control, as shown in Figure 6. In our case, the main goal of MPC is to minimize the error between the predicted outputs and the set points. Then, we build a cost function which measures the squared error between the predicted outputs and the set points as follows.

$$\begin{aligned} J &= J_{MPC}(\theta_m(k), \theta_m(k+1)) \quad (8)\\ &= (x_p(k+1|k-1) - x_r(k+1))^2 \\ &+ (y_p(k+1|k-1) - y_r(k+1))^2 \\ &+ (x_p(k+2|k-1) - x_r(k+2))^2 \\ &+ (y_p(k+2|k-1) - y_r(k+2))^2, \end{aligned}$$

where $(x_r(k+1), y_r(k+1))$ and $(x_r(k+2), y_r(k+2))$ are the set points derived from the path generation method; $\theta_m(k)$ and $\theta_m(k+1)$ are the predicted inputs, which are the magnetic field angles; $(x_p(k+1|k-1), y_p(k+1|k-1))$ and

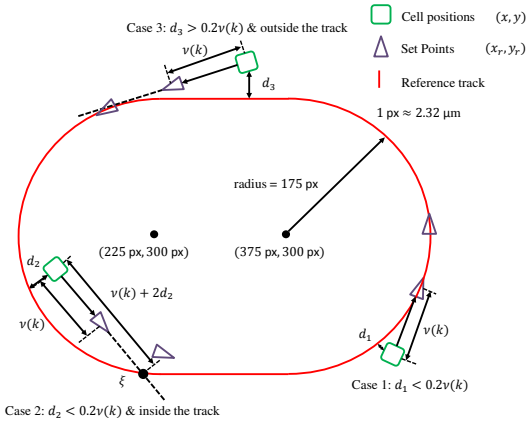

Fig. 5: The reference track and the method to generate the set points in the three different cases. In this picture, the green squares represent the cell positions; the purple triangles represent the set points; $\nu(k)$ is the cell position distance between two consecutive sampling time; d_1, d_2, and d_3 are the distances between *T. pyriformis* and the reference track; ξ is a dot in the reference track with distance $\nu(k) + 2d_2$ to the cell position.

$(x_p(k+2|k-1), y_p(k+2|k-1))$ are the predicted outputs, which are the predicted cell positions with error offset.

$$x_p(k+i|k-1) = x(k+i|k-1) + x_e(k+i|k-1), \quad (9)$$
$$y_p(k+i|k-1) = y(k+i|k-1) + y_e(k+i|k-1), \quad (10)$$

for $i = 1, 2$, where $(x(k+1|k-1), y(k+1|k-1))$ and $(x(k+2|k-1), y(k+2|k-1))$ are the predicted positions without error offset, which are derived by Equations (2)-(4) based on the measurement of the $k-1$ step cell position $(x(k-1), y(k-1))$; the predicted plant model errors, $(x_e(k+1|k-1), y_e(k+1|k-1))$ and $(x_e(k+2|k-1), y_e(k+2|k-1))$, are considered to be constant. That is, for $i = 1, 2$,

$$x_e(k+i|k-1) = x_e(k|k-1) = x(k) - x(k|k-1), \quad (11)$$
$$y_e(k+i|k-1) = y_e(k|k-1) = y(k) - y(k|k-1), \quad (12)$$

where $(x(k), y(k))$ is the k step cell position; $(x(k|k-1), y(k|k-1))$ is the k step predicted position without error offset. Note that this technique of compensating for the plant model error is proposed in [18].

Because the cost function $J_{MPC}(\theta_m(k), \theta_m(k+1))$ is a non-convex function, we find a small enough local minimum substitutes for the global minimum. From Equation (2), we find that the cost function is a $2\pi \times 2\pi$ periodic function with respect to $\theta_m(k)$ and $\theta_m(k+1)$. So the global minimum should appear on the domain $-\pi \leq \theta_m(k) \leq \pi$ and $-\pi \leq \theta_m(k+1) \leq \pi$. We then define a grid search to find the local minima on this domain. We create a 8×8 grid on the $2\pi \times 2\pi$ domain and execute the Newton Iteration method to search

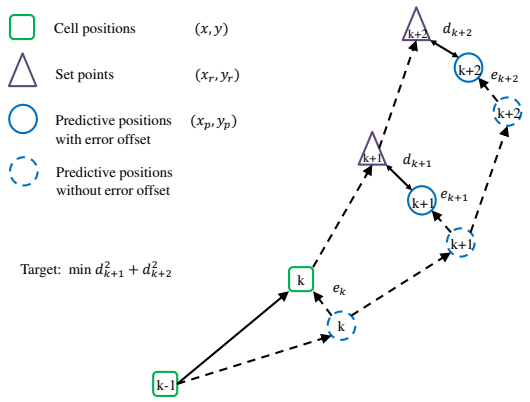

Fig. 6: Main idea of MPC. In this picture, k is the time step; the green squares represent the cell positions, which are $(x(k-1), y(k-1))$ and $(x(k), y(k))$; the purple triangles represent the set points, which are $(x_r(k+1), y_r(k+1))$ and $(x_r(k+2), y_r(k+2))$; the blue dash circles represent the predicted positions without error offset, which are $(x(k|k-1), y(k|k-1))$, $(x(k+1|k-1), y(k+1|k-1))$, and $(x(k+2|k-1), y(k+2|k-1))$; the blue solid circles represent the predicted positions with error offset, which are $(x_p(k+1|k-1), y_p(k+1|k-1))$ and $(x_p(k+2|k-1), y_p(k+2|k-1))$; d_{k+1} and d_{k+2} are the distances between the predicted positions with error offset and the set points; e_k, e_{k+1}, and e_{k+2} are the plant model errors.

the local minima starting from each of the 49 intersections.

$$\Theta_{n+1} = \Theta_n - \left[\frac{\partial^2 J_{MPC}(\Theta_n)}{\partial \Theta_n^2}\right]^{-1} \frac{\partial J_{MPC}(\Theta_n)}{\partial \Theta_n}, \quad (13)$$

where $\Theta_n = [\theta_m^n(k), \theta_m^n(k+1)]^T$; n is the Newton Iteration step; k is the time step; $\theta_m(k)$ and $\theta_m(k+1)$ are the magnetic field angles.

To ensure the stability of the system, a finer partition can be used. However, it will increase the calculation time. On the other hand, from both the simulation and experimental results, the 8×8 grid has been shown to result in a good tracking performance.

In summary, the MPC algorithm is presented in Algorithm 1.

V. RESULT & COMPARISON

In the experiment, a single *T. pyriformis* cell is manually controlled for 10 seconds to get enough data for plant model identification. Then, the parameters a_0 and b_0 are computed based on the BLS method. Next, we manually manipulate *T. pyriformis* to the starting point (275 px, 128 px) with 1 px $\approx$ 2.32 μm to enable the feedback control. Finally, the feedback control with MPC algorithm is executed for about 7.5 seconds, as shown in Figure 7. The magnetic field strength is set to be 2 mT. We then show the simulation result by Matlab in Figure 8.

Algorithm 1 Coding process of MPC algorithm

1: Compute a_0 and b_0 based on the captured manual control data.
2: **for** $k = 1, 2, 3, \ldots$ **do**
3: Get $(x(k), y(k))$ from image processing.
4: Calculate $\nu(k)$ by averaging previous 10 steps' cell velocity.
5: Compute $\theta_t(k)$ by Equations (3)-(4) which satisfies $\theta_t(k) \in [\theta_t(k-1) - \pi, \theta_t(k-1) + \pi]$.
6: Calculate $(x(k|k-1), y(k|k-1))$, $(x(k+1|k-1), y(k+1|k-1))$, and $(x(k+2|k-1), y(k+2|k-1))$ based on Equations (2)-(4) and $(x(k-1), y(k-1))$.
7: Compute the plant model error $x_e(k|k-1) = x(k) - x(k|k-1)$, $y_e(k|k-1) = y(k) - y(k|k-1)$.
8: Generate $k+1$ and $k+2$ steps set points, $(x_r(k+1), y_r(k+1))$ and $(x_r(k+2), y_r(k+2))$, based on the k step cell position and the path generation method.
9: Predict future two steps cell positions with error offset, $(x_p(k+1|k-1), y_p(k+1|k-1))$ and $(x_p(k+2|k-1), y_p(k+2|k-1))$ based on Equations (9)-(10).
10: Build cost function $J_{MPC}(\theta_m(k), \theta_m(k+1))$ to measure the error between predicted positions with error offset and set points in $k+1$ and $k+2$ steps.
11: Use the Newton Iteration method from different initial values on the domain to find the small enough local minimum $(\theta_m(k), \theta_m(k+1))$, which substitutes for the global minimum of the cost function.
12: Exert $\theta_m(k)$ to the plant.
13: **end for**

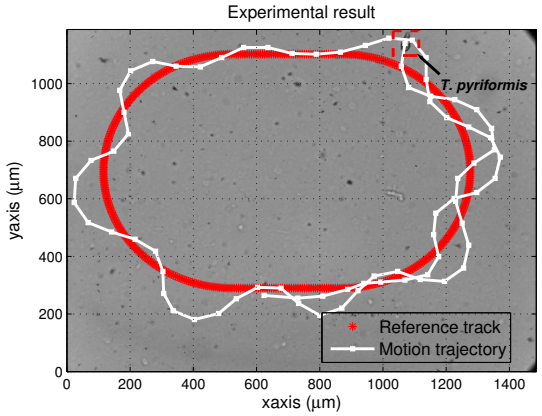

Fig. 7: Experimental result. In this picture, the red stars represent the reference track; the green square line is the *T. pyriformis* motion trajectory.

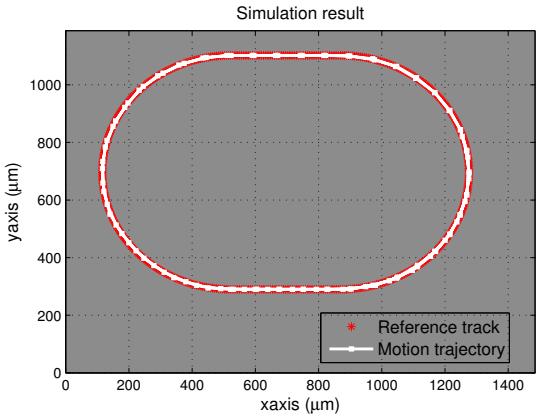

Fig. 8: Simulation result. In this picture, the red stars represent the reference track; the green square line is the *T. pyriformis* motion trajectory.

We can clearly observe that the MPC algorithm performs well in simulation, achieving practically perfect tracking performance. The experimental result also shows that the cell indeed tracks the reference trajectory. However, the level of tracking error in the experiment is significantly worse than the simulation. In the next section, we formulate a hypothesis on how we can improve the performance of the feedback controller.

VI. CONCLUSION AND FUTURE WORKS

In this paper, we discuss the use of MPC in the motion control of the magnetotactic *T. pyriformis*. The magnetotactic *T. pyriformis* is created by introducing artificial magnetic dipoles in the cell. Our control input is the direction of an external magnetic field, which is kept at a constant intensity. Based on the mechanical analysis of the magnetotactic *T. pyriformis* under the influence of the external magnetic field, a discrete-time plant model is generated. The plant model parameters are calculated by using the BLS method. We then formulate a feedback control algorithm, based on MPC, to make *T. pyriformis* follow a reference track. Finally, we evaluate the feedback control performance using the numerical simulation and experiment.

As seen in the previous section, the feedback control algorithm works very well in theory (as shown by the simulation result). However, there is a performance gap between the simulation and experimental result. We hypothesize that this difference is due to two factors, (i) external disturbance, (ii) systematic modelling error. In the future, we plan on conducting more comprehensive experiments that will allow us to better characterize the external disturbance affecting the system. For example, by manually controlling the cell to follow a straight line, and measuring the deviation of the cell trajectory from a straight line. We will also identify the image processing and computation delay. A significant delay could be the reason behind the performance drop of the feedback controller in the experiment.

VII. ACKNOWLEDGMENTS

This work is partially supported by NSF CMMI Control Systems (Award #1000284).

REFERENCES

[1] B. R. Donald, C. G. Levey, and I. Paprotny, "Planar Microassembly by Parallel Actuation of MEMS Microrobots," Microelectromechanical Systems, Journal of, vol. 17, no. 4, pp. 789–808, 2008.

[2] I. W. Hunter, S. Lafontaine, P. M. F. Nielsen, P. J. Hunter, and J. M. Hollerbach, "Manipulation and dynamic mechanical testing of microscopic objects using a tele-micro-robot system," Control Systems Magazine, IEEE, vol. 10, no. 2, pp. 3–9, 1990.

[3] T. G. Leong, C. L. Randall, B. R. Benson, N. Bassik, G. M. Stern, and D. H. Gracias, "Tetherless thermobiochemically actuated microgrippers," vol. 106, no. 3, 2009.

[4] C. Pawashe, S. Floyd, and M. Sitti, "Multiple magnetic microrobot control using electrostatic anchoring," Applied Physics Letters, vol. 94, no. 16, p. 164108, 2009.

[5] A. A. Julius, M. S. Sakar, E. Steager, U. K. Cheang, M. J. Kim, V. Kumar, and G. J. Pappas, "Harnessing bacterial power in microscale actuation," in Robotics and Automation, 2009. ICRA '09. IEEE International Conference on, 2009, pp. 1004 –1009.

[6] S. Martel, C. C. Tremblay, S. Ngakeng, and G. Langlois, "Controlled manipulation and actuation of micro-objects with magnetotactic bacteria," Applied Physics Letters, vol. 89, no. 23, p. 233904, 2006.

[7] B. Behkam and M. Sitti, "Bacterial flagella-based propulsion and on/off motion control of microscale objects," Applied Physics Letters, vol. 90, no. 2, pp. 1–3, 2007.

[8] A. Itoh, "Motion control of protozoa for bio-MEMS," Mechatronics, IEEE/ASME Transactions on, vol. 5, no. 2, pp. 181 –188, 2000.

[9] R. S. Fearing, "Control of a Micro-Organism as a Prototype Micro-Robot," 2nd Int. Symp. on Micromachines and Human Schiences., 1991.

[10] D. B. Weibel, R. Garstecki, D. Ryan, W. R. DiLuzio, M. Mayer, J. E. Seto, and G. M. Whitesides, "Microoxen: Microorganisms to move microscale loads," Proceedings of The National Academy of Sciences, vol. 102, no. 34, pp. 11 963–11 967, 2005.

[11] A. Itoh, W. Tamura, and T. Mishima, "Motion Control of Euglena Group by Weak Laser Scanning System and Object Manipulation Using Euglena Group," pp. 43–47, 2005.

[12] D. H. Kim, D. Casale, L. Köhidai, and M. J. Kim, "Galvanotactic and phototactic control of *Tetrahymena pyriformis* as a microfluidic workhorse," Applied Physics Letters, vol. 94, no. 16, p. 163901, 2009.

[13] D. H. Kim, S. Brigandi, A. A. Julius, and M. J. Kim, "Real-time feedback control using artificial magnetotaxis with rapidly-exploring random tree (RRT) for *Tetrahymena pyriformis* as a microbiorobot," in Robotics and Automation (ICRA), 2011 IEEE International Conference on, may 2011, pp. 3183 –3188.

[14] E. G. Carlos, M. P. David, and M. Manfred, "Model predictive control: Theory and practice–A survey," Automatica, vol. 25, no. 3, pp. 335 – 348, 1989.

[15] D. H. Kim, U. K. Cheang, L. Köhidai, D. Byun, and M. J. Kim, "Artificial magnetotactic motion control of *Tetrahymena pyriformis* using ferromagnetic nanoparticles: A tool for fabrication of microbiorobots," Applied Physics Letters, vol. 97, no. 17, pp. 173 702 –173 702–3, 2010.

[16] J. L. Rifkin and R. Ballentine, "Magnetic Fettering of the Ciliated Protozoon *Tetrahymena pyriformis*," Transactions of the American Microscopical Society, vol. 95, no. 2, pp. 189–197, 1976.

[17] P. A. Ioannou and J. Sun, Robust Adaptive Control. Prentice Hall PTR, 1995.

[18] E. F. Camacho and C. Bordons, Model Predictive Control. Springer, 2007.